

Low-temperature Magnetic Fluctuations Investigated by ^{125}Te -NMR on the Uranium-based Superconductor UTe_2

Hiroki Fujibayashi^{1*}, Katsuki Kinjo^{1†}, Genki Nakamine¹, Shunsaku Kitagawa¹, Kenji Ishida^{1‡}, Yo Tokunaga², Hironori Sakai², Shinsaku Kambe², Ai Nakamura³, Yusei Shimizu³, Yoshiya Homma³, Dexin Li³, Fuminori Honda³, and Dai Aoki^{3,4}

¹Department of Physics, Kyoto University, Kyoto 606-8502, Japan

²Advanced Science Research Center, Japan Atomic Energy Agency, Tokai, Ibaraki 319-1195, Japan

³IMR, Tohoku University, Oarai, Ibaraki 311-1313, Japan

⁴University Grenoble, CEA, IRIG-PHERIQS, F-38000 Grenoble, France

To investigate the static and dynamic magnetic properties on the uranium-based superconductor UTe_2 , we measured the NMR Knight shift K and the nuclear spin-lattice relaxation rate $1/T_1$ in $H \parallel a$ by ^{125}Te -NMR on a ^{125}Te -enriched single-crystal sample. $1/T_1T$ in $H \parallel a$ is much smaller than $1/T_1T$ in $H \parallel b$ and c , and magnetic fluctuations along each axis are derived from the $1/T_1T$ measured in H parallel to all three crystalline axes. The magnetic fluctuations are almost identical at two Te sites and isotropic at high temperatures, but become anisotropic below 40 K, where heavy-fermion state is formed. The character of magnetic fluctuations in UTe_2 is discussed with the comparison to its static susceptibility and the results on other U-based superconductors. It is considered that the magnetic fluctuations probed with the NMR measurements are determined by the magnetic properties inside the two-leg ladder formed by U atoms, which are dominated by the $q_a = 0$ ferromagnetic fluctuations.

Superconductivity in UTe_2 [Superconducting (SC) transition temperature $T_{\text{SC}} = 1.6$ K] was discovered at the end of 2018,¹⁾ and was confirmed by other group immediately.²⁾ UTe_2 has the orthorhombic crystal structure with the space group $Immm$ (#71, D_{2h}^{25}), which belongs to the symmorphic group [Fig.1(a)].³⁾ UTe_2 is considered to be a spin-triplet superconductor because its characteristic SC properties, such as extremely high SC upper critical fields H_{c2} ^{1,4)} and the magnetic-field (H) enhancement of H_{c2} ,¹⁾ are quite similar to those observed in uranium (U)-based ferromagnetic (FM) superconductors⁶⁾ (UGe_2 under pressure,⁷⁾ and URhGe ⁸⁾ and UCoGe ⁹⁾ at ambient pressure), which are spin-triplet superconductors. However, different from these FM superconductors, UTe_2 shows superconductivity in the paramagnetic state, and does not show any FM ordering even in the high-pressure region where superconductivity suddenly disappears.^{10,11)} More surprisingly, inelastic neutron scattering (INS) experiments have revealed the predominance of the incommensurate antiferromagnetic (AFM) spin fluctuations with the wave-vector $\mathbf{Q}_{\text{ic}} = (0, 0.57, 0)$.^{12,13)} Since the U atoms in UTe_2 form a two-leg ladder with legs along the a axis and rungs along the c axis [Fig. 1(a)], the AFM interaction is parallel to the inter two-leg ladder direction along the b axis. Thus, one of the great interests in UTe_2 is to understand the magnetic properties in the normal state, particularly whether FM fluctuations exist or not inside the two-leg ladder structure above T_{SC} , although the INS measurements could not detect any FM fluctuations.^{12,13)} To clarify this issue, ^{125}Te -NMR measurements for $H \parallel a$ on a single-crystal UTe_2 are crucially important, because the directional magnetic fluctuations can be known as discussed later.

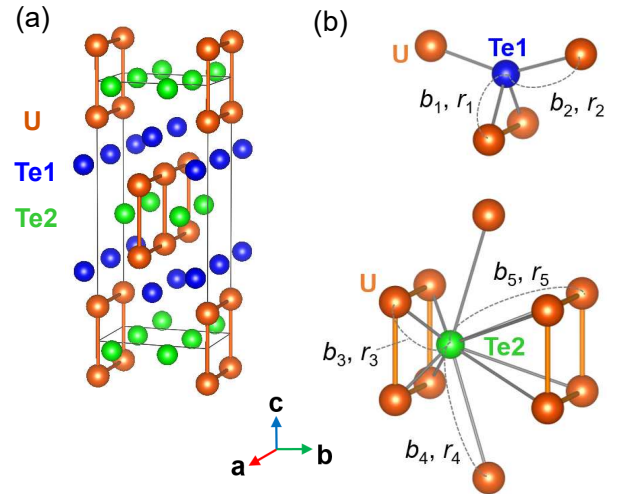


Fig. 1. (Color online) Crystal structure of UTe_2 emphasizing the two-leg ladder structure formed by the U atoms. Two crystallographically inequivalent Te sites, $4j$ and $4h$, with the point symmetries $mm2$ and $m2m$ are shown as Te1 and Te2, respectively.³⁾ (b) Atomic arrangement around each Te site. b_j s and r_j s indicate the transfer-field parameters and the distances between U and Te site, respectively. Here, $r_1 = 3.0553$ Å, $r_2 = 3.1817$ Å, $r_3 = 3.1648$ Å, $r_4 = 5.2706$ Å, and $r_5 = 5.3462$ Å.⁵⁾

In the previous measurement,¹⁴⁾ we could not observe ^{125}Te -NMR signals in $\mu_0 H \sim 2$ T below 20 K for $H \parallel a$ due to the divergence of the nuclear spin-spin relaxation rate $1/T_2$ and the broadening of the spectrum. To overcome this difficulty, we prepared a ^{125}Te -enriched single crystal sample with a nearly cubic shape, and successfully observed the ^{125}Te -NMR signals in low fields parallel to the a axis. We measured the NMR Knight shift K and nuclear spin-lattice relaxation rate $1/T_1$ under magnetic field in $H \parallel a$ down to 1.5 K. Together with previous NMR results,¹⁴⁾ magnetic fluctuations along each crystalline axis are derived. It was found

*fujibayashi.hiroki.w49@kyoto-u.ac.jp

†Present address: Institute of Multidisciplinary Research for Advanced Materials, Tohoku University, Sendai, Miyagi 980-8577, Japan

‡kishida@scphys.kyoto-u.ac.jp

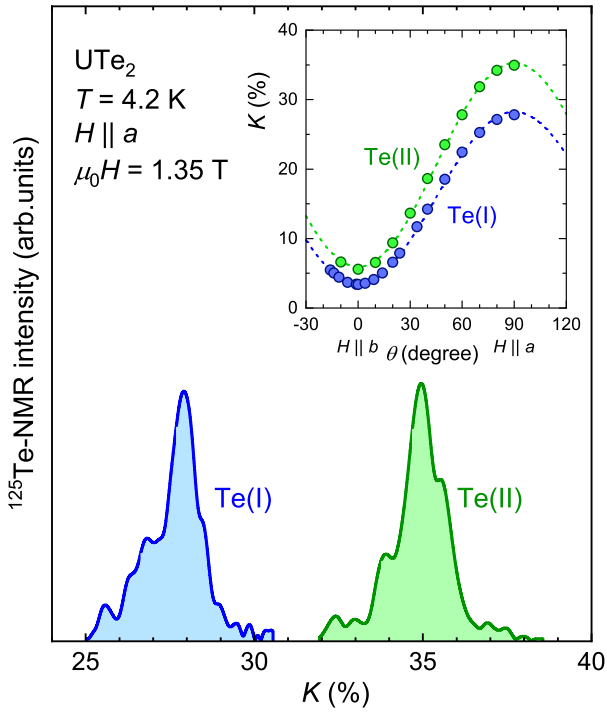


Fig. 2. (Color online) ^{125}Te -NMR spectrum in $H \parallel a$ shown against the Knight shift of $K = (f - f_0)/f_0$. The smaller [larger]- K peak is denoted as a Te(I) [Te(II)] peak. The inset shows the magnetic-field angle dependence of the Te(I) and Te(II) peaks in the ab plane.

that magnetic fluctuations are almost isotropic at high temperatures, and becomes highly anisotropic below 40 K, as in the case of the static susceptibility.

Single-crystal UTe_2 was grown by the chemical-vapor-transport method with iodine as the transport agent.^{1,2)} Natural U and 99.9% ^{125}Te -enriched metals were used as starting materials for the present sample. The ^{125}Te (nuclear spin $I = 1/2$, gyromagnetic ratio $^{125}\gamma_n/2\pi = 13.454$ MHz/T)-NMR measurements were performed on a single crystal of $0.8 \times 1.2 \times 0.9$ mm³ size. The frequency-sweep NMR spectrum was obtained using the Fourier transform of a spin-echo signal observed after the spin-echo radio-frequency pulse sequence with a 5-kHz step in a fixed magnetic field. The magnetic field was calibrated using ^{63}Cu ($I = 3/2$, $^{63}\gamma/2\pi = 11.285$ MHz/T) and ^{65}Cu ($I = 3/2$, $^{65}\gamma/2\pi = 12.089$ MHz/T) NMR signals arising from the NMR coil. We used the split SC magnet, which generates a horizontal field, and combined it with a single-axis rotator to apply a magnetic field in each crystalline direction precisely.

Figure 2 shows the ^{125}Te -NMR spectra for $H \parallel a$, which are shown against the NMR shift $K = (f - f_0)/f_0$. Here, f is the NMR frequency, and f_0 is the reference frequency determined as $f_0 = (^{125}\gamma_n/2\pi)\mu_0H$. There are two crystallographically inequivalent Te sites, $4j$ and $4h$, with the point symmetries $mm2$ and $m2m$ in UTe_2 , and these are denoted as Te1 and Te2 sites [Fig. 1(a)], respectively. Correspondingly, we observed two ^{125}Te -NMR peaks as reported in the previous paper.^{15–17)} An NMR peak with the smaller [larger] K in $H \parallel b$ is assigned as Te(I) [Te(II)] by following the previous paper.¹⁴⁾ The inset of Fig. 2 shows the H angular dependence of the NMR Knight shift at both the Te(I) and Te(II) peaks measured in the ab plane at 4.2 K. These angle dependence are well fitted by the

Table I. Hyperfine coupling constants A_{hf}^α evaluated from the linear relation between Knight shift and bulk susceptibility along $\alpha = a, b$ and c . This corresponds to the diagonal term in the hyperfine tensor.

	$H \parallel a$	$H \parallel b$	$H \parallel c$
	A_{hf}^a (T/ μ_B)	A_{hf}^b (T/ μ_B)	A_{hf}^c (T/ μ_B)
Te(I)	3.8	3.4	3.9
Te(II)	4.7	5.2	3.9

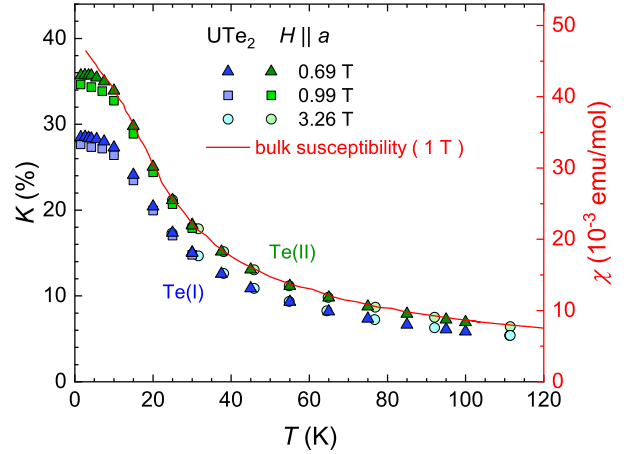


Fig. 3. (Color online) Temperature dependence of the Knight shift determined from the Te(I) and Te(II) peaks. The K_a above 30 K¹⁴⁾ and χ_a above 5 K¹⁸⁾ are quoted from the references.

theoretical curves of $K(\theta) = K_a \sin^2 \theta + K_b \cos^2 \theta$, where K_a (K_b) is the Knight shift in $H \parallel a$ (b). The a -axis aligned NMR spectra of the Te(I) and Te(II) peaks were detected by following the angle dependence in the ab plane from the observed b -axis NMR spectra.^{14–17)} K_a of the Te(I) and Te(II) peaks at 4.2 K is 27.9% and 35.2%, respectively. In the present measurement, the smaller magnetic field of $\mu_0H = 1.35$ T than in the previous study¹⁴⁾ makes the NMR peak sharper.

From the present measurement, it turned out that the previous NMR-peak assignment in $H \parallel a$ should be reinterpreted. Although the Te(I) and Te(II) peaks were overlapped in $H \parallel c$ in the previous study,¹⁴⁾ there are found to be no crossing nor overlapping in the angle dependence of the two peaks in the present study. The present peak assignment results in nearly isotropic values of the hyperfine coupling constants at the two Te sites, as shown in Table I. Note that the peak assignment presented here [Te(I) and Te(II)] does not correspond to the crystallographical site (Te1 and Te2).

Figure 3 shows the temperature (T) dependence of K_a measured in 0.69 and 0.99 T below 100 K. In the figure, the K_a data measured in 3.26 T above 30 K¹⁴⁾ and the χ_a measured in 1 T are also shown.¹⁸⁾ As reported in the paper,¹⁹⁾ the K_a is proportional to χ_a above 10 K, but is nearly saturated and remains almost constant at low temperatures. This is in contrast to the continuous increase in χ_a below 10 K, which would be ascribed to the extrinsic effect induced by the U-atom deficiency.²⁰⁾

Figures 4(a)–(c) show the T dependence of $1/T_1T$ of Te(I) and Te(II) measured in H parallel to each crystalline axis, respectively. $1/T_1T$ in all directions of Te(I) and Te(II) roughly follows the Curie-Weiss behavior with different Curie terms

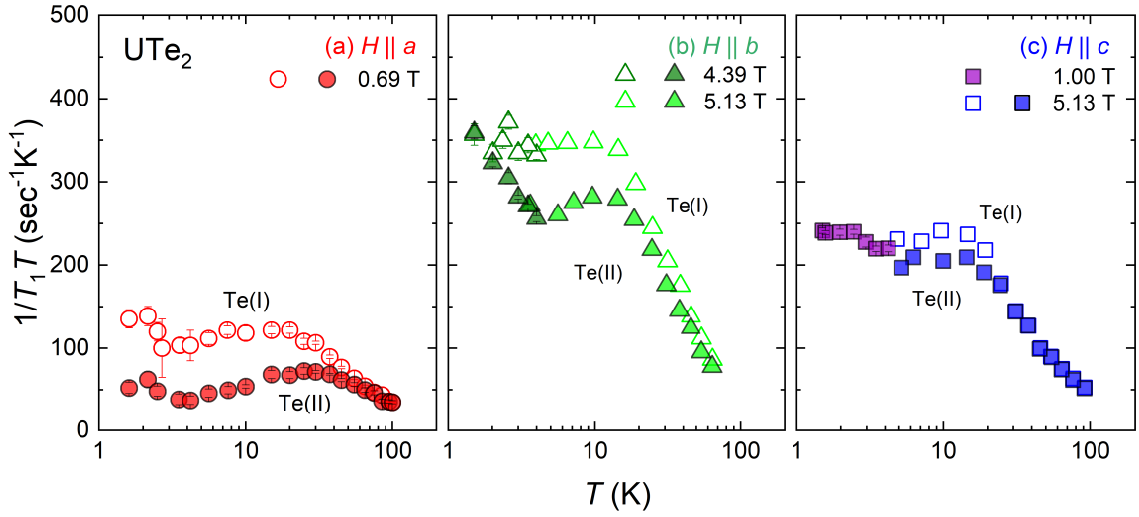


Fig. 4. (Color online) Temperature dependence of $1/T_1T$ at Te(I) and Te(II) in (a) $H \parallel a$, (b) $H \parallel b$ and (c) $H \parallel c$. The data of $1/T_1T$ in $H \parallel b$ and $H \parallel c$ above 4.2 K are quoted from the reference.¹⁴ $1/T_1T$ in $H \parallel c$ below 4.2 K was measured at the broad NMR peak arising from the Te(I) and Te(II) signals.

above 45 K, which is consistent with the resistivity behavior, suggestive of the localized $5f$ state. With decreasing T , all $1/T_1T$ s deviate from the Curie-Weiss behavior and almost saturate below 15 K in $H \parallel b$ and c . This temperature might be related to a broad Schottky-like anomaly observed at ~ 12 K with the various thermodynamic, transport probes²¹) and the nuclear spin-spin relaxation rate $1/T_2$.¹⁹) In contrast, $1/T_1T$ in $H \parallel a$ shows a broad maximum at around 20 K for Te(I) and 30 K for Te(II), respectively. The magnitude of $1/T_1T$ at low T is different between Te(I) and Te(II) in $H \parallel a$ and b , but the difference is small in $H \parallel c$. Below 4 K, $1/T_1T$ increases again. This increase is stronger at Te(II), and would be relevant to the low- T increase reported in the relaxation rate in the μ SR²²) and $1/T_2$.¹⁹)

Following the previous procedure,¹⁴) we derived the directional dynamic susceptibility components $R_{i,\alpha}$ for Te(i) along each orthorhombic crystal axis α with using the relation of $(1/T_1T)_{i,\gamma} = R_{i,\alpha} + R_{i,\beta}$. Here, $i = \text{I and II}$, $\alpha, \beta, \gamma = \{a, b, c\}$, and $(1/T_1T)_{i,\gamma}$ is the $1/T_1T$ of Te(i) measured in $H \parallel \gamma$. In general, $R_{i,\alpha}$ is expressed as

$$R_{i,\alpha} = \sum_{\mathbf{q}, \xi} A_i^{\alpha\xi}(\mathbf{q})^2 \frac{\chi''_{\xi}(\mathbf{q}, \omega_N)}{\omega_N}. \quad (1)$$

with the ω_N and $\chi''_{\xi}(\mathbf{q}, \omega_N)$ are the NMR frequency and the imaginary part of the dynamic susceptibility along $\xi = \{a, b, c\}$, respectively. $A_i^{\alpha\xi}(\mathbf{q})$ is a \mathbf{q} -dependent hyperfine coupling tensor at Te(i), which is assumed to be expressed as $A_i^{\alpha\xi}(\mathbf{q})^2 \sim |A_i^{\alpha\xi}(0)F_i(\mathbf{q})|^2$ with $F_i(\mathbf{q}) = \sum_j b_j e^{i\mathbf{q}\cdot\mathbf{r}_j}$ for simplicity. Here, $F_i(\mathbf{q})$ is the site-dependent form factor, which consists of the transfer-field parameters b_j from the j th-U atoms surrounding the Te(i) as shown in Fig. 1 (b), and this acts as the filter of spin fluctuations.

Figures 5(a)-(c) show the T dependence of $R_{i,\alpha}$ derived from $1/T_1T$ of Te(I) and Te(II) signals with the above relations. The magnitude and temperature dependence of $R_{i,\alpha}$ are almost the same between two signals, although the magnitude of R_c at low temperatures is different. In addition, it was found that the anisotropy of $R_{i,\alpha}$ becomes remarkable below

40 K where the χ along the b axis shows a maximum. This temperature is called $T_{\chi_{\max}}$ and is regarded as the formation of the heavy-fermion state. $1/T_1T$ results also show that the anisotropic heavy-fermion state is formed, consistent with the Knight-shift results.

Here, we consider the effect of AFM fluctuations along the b axis detected by the INS measurements with $\mathbf{Q} = (0, q_b, 0)$.^{12,13}) As seen in Fig. 1(b), the Te1 site is located at the center of the above two U atoms along the b axis and the bottom two U atoms along the a axis. The Te2 sites are at the nonsymmetric position in the unit cell, and thus, $1/T_1T$ at the Te2 site can also probe the AFM fluctuations. The form factor at the Te x ($x = 1$ and 2) site against q_b along $(0, q_b, 0)$ $F_x(q_b)$ is calculated in the presence of the three-dimensional coupling as,²³)

$$\begin{aligned} |F_1(q_b)|^2 &= 4b_1^2 + 4b_2^2 \cos^2(q_b/2) + 8b_1b_2 \cos(q_b/2) \\ |F_2(q_b)|^2 &= 16 \left[|b_3 - b_5|^2 + 4b_3b_5 \cos^2(q_b/2) \right] \\ &\quad + 4b_4^2 + 16(b_3b_4 + b_4b_5) \cos(q_b/2). \end{aligned}$$

As for the form factor of the Te2 site, the second and third nearest neighbor U sites are taken into account. As the distances between the Te1 site and the surrounding four U atoms (r_1 and r_2) are almost the same, we assumed that the b_1 and b_2 are the same ($b_1 = b_2$). At the Te2 site, as $r_4 \sim r_5$, we assumed $b_4 = b_5$. $b_3/b_{4(5)}$ is the ratio of the hyperfine coupling constants for the nearest and second (third) nearest-neighbor sites at the Te2 site, and are estimated as $\sim (r_{4(5)}/r_3)^3 \sim 4.7$ by assuming the Ruderman-Kittel-Kasuya-Yosida type interaction.²³)

Figure 6 shows the q_b -dependent form factor $|F_x(q_b)|^2$, where each $\sum_{q_b} |F_x(q_b)|^2$ is normalized to the unit. It is noted that the q_b dependence of $|F_x(q_b)|^2$ is different between two sites, and thus, T dependence of $1/T_1T$ should be different between two Te sites in general, as the site difference of $|F_x(q_b)|^2$ yields the difference of $\sum_{q_b} |F_x(q_b)|^2 \chi''(\mathbf{q}, \omega_N)$. The difference is mainly due to the presence of the third term in $|F_1(q_b)|^2$, which arises from the c -axis interladder coupling. However, the INS measurements revealed that the interladder magnetic

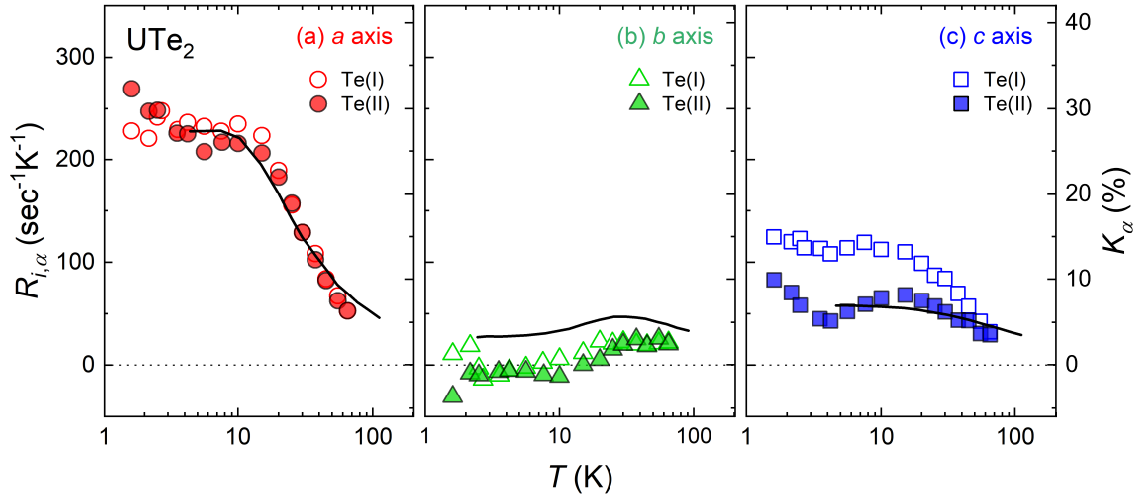


Fig. 5. (Color online) Temperature dependence of (a) $R_{i,a}$, (b) $R_{i,b}$, and (c) $R_{i,c}$ ($i = \text{I and II}$) evaluated from the data shown in Fig. 4. Temperature dependence of K_{α} ($\alpha = a, b, \text{ and } c$) at Te(I) is also shown by the solid curves¹⁴⁾

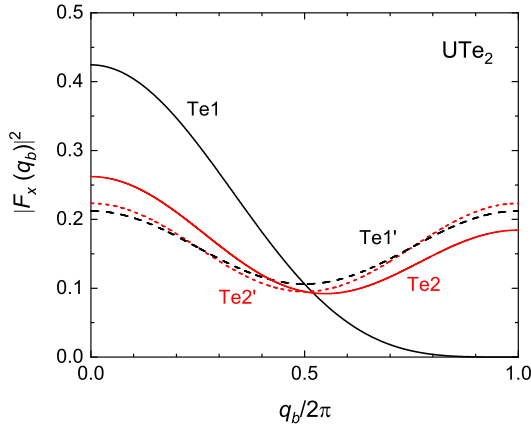


Fig. 6. (Color online) q_b dependence of the hyperfine form factor $|F_x(q_b)|^2$ at the Te1 and Te2 sites. The dotted curves (Te1' and Te2') are the q_b dependence of $|F_x(q_b)|^2$, which are the Te1 and Te2 form factor without the c -axis interladder coupling. Each form factor is normalized to be $\sum_{q_b} |F_x(q_b)|^2 = 1$.

coupling along the c axis is negligibly weak, and the AFM coupling along the b axis would induce the frustration in the magnetic coupling along the c axis. Thus, it is reasonable to neglect the interladder magnetic coupling along the c axis. In this case, the terms related to the c -axis interladder correlation ($8b_1b_2 \cos(q_b/2)$ and $16(b_3b_4 + b_4b_5) \cos(q_b/2)$) become zero. Thus, the form factor at Te1 and Te2 sites are expressed as,

$$|F_{1'}(q_b)|^2 = 4b_1^2 + 4b_2^2 \cos^2(q_b/2)$$

$$|F_{2'}(q_b)|^2 = 16[b_3 - b_5]^2 + 4b_3b_5 \cos^2(q_b/2) + 4b_4^2.$$

The q_b -dependence of the above form factors at the Te1 and Te2 sites is shown by the dotted curves (Te1' and Te2') in Fig. 6, which are quite similar to each other. Therefore, the AFM fluctuations with $q_b \sim 0.57$ observed with the INS measurements^{12,13)} are detectable in the same manner with $1/T_1T$ at both the sites. The similar $1/T_1T$ behavior at Te(I) and Te(II) are interpreted with the absence of the interladder magnetic coupling along the c axis.

To investigate the properties of the magnetic fluctuations, $R_{i,\alpha}$ is compared with K_{α} at Te(I), as shown in Figs. 5(a)-(c). Almost linear relations between $R_{i,\alpha}$ and K_{α} are observed. This indicates that the diagonal component in the hyperfine coupling tensor is dominant in the a axis. It is noted that K_a and R_a continue to increase even below $T_{\chi_{\max}}$, where U-5f electron is in the itinerant regime. This implies that the most dominant contributions in $\chi_a''(q, \omega)$ is $\chi_a''(0, 0)$, indicative of the dominance of the $q_a = 0$ fluctuations. This seems consistent with the INS result that the nearest U atoms have in-phase correlations.¹³⁾ It is suggested that the fluctuations detected with the NMR measurement would be confined in the low-energy regions ($\sim 10^{-4}$ meV), since the appreciable FM fluctuations are not detected with the INS measurements above 0.7 meV.¹²⁾ We also point out that the T dependence of the incommensurate AFM fluctuations is almost the same as that of $\chi(0)$.¹³⁾ This implies that the magnetic fluctuations might be q independent at the low-energy region. This indicates that the local-moment character might remain even below $T_{\chi_{\max}}$. It is important to investigate the energy dependence of the magnetic fluctuations to make clear the relation between NMR and INS results.

In contrast, R_b is smaller than K_b and almost zero below 10 K at Te(I) and Te(II). This indicates that the magnetic fluctuations are absent along the b direction at low T , although the static spin component is finite in the whole T range. Furthermore, the R_c at Te(I) is significantly larger than K_c , although R_c at Te(II) is almost the same as K_c at Te(II). This suggests the presence of the additional R_c , which is related to the off-diagonal component in the hyperfine coupling tensor at Te(I). Since the Te2 site is located at the symmetric position with respect to the two-leg-ladder chain, in which the U atoms have the in-phase correlations,¹³⁾ it is considered that the Te2 site does not have off-diagonal components in the hyperfine coupling tensor. One possibility is that the average effective field along the c axis can arise, when the U electronic spins near the Te1 site are aligned to the a or b axis with the incommensurate AFM coupling along the b axis, and that the fluctuations of the c -axis effective field can induce the additional R_c . The difference of R_c values of the Te(I) and Te(II) peaks might give

useful information about the NMR-signal assignment arising from the two Te sites. Recently, it was reported that low- T $1/T_1T$ in $H \parallel b$ for the two Te sites becomes different by applying pressure (P), and that $1/T_1T$ of Te(I) is more enhanced than $1/T_1T$ of Te(II), which is clearly recognized near critical pressure.²⁴⁾ Since the low- T magnetic susceptibility along the b axis (χ_b) increases with P ,¹⁸⁾ the enhancement of $1/T_1T$ in $H \parallel b$ of Te(I) might be understood by the increase of R_c with the above scenario.

Finally, we compare the present results to those observed in other U-based compounds. In the U-based heavy-fermion superconductors such as URu₂Si₂,²⁵⁾ UPt₃,²⁶⁾ and UPd₂Al₃,²⁷⁾ U-5 f electrons show the crossover from high- T localized to the low- T heavy-fermion states, as observed in UTe₂. In these compounds, AFM fluctuations appear to be responsible for the crossover process and dominate the low-frequency magnetic properties. The presence of the AFM fluctuations is recognized from the comparison of the T dependence between R_a and K_a , and the development of R_a is much larger than that of K_a with decreasing T . On the other hand, as discussed above, R_a is well scaled to K_a even below $T_{\chi_{\max}}$ down to the lowest T in UTe₂. This is quite in contrast with the behavior observed in these compounds, and reminiscences the FM SC UCoGe^{28,29)} and nearly FM UCoAl.³⁰⁾ Our NMR results in UTe₂ would be dominated by the magnetic properties inside the two-leg ladder formed by the U atoms, since the two Te sites are located in the vicinity of the ladder.

In summary, we observed the a -axis NMR signals down to 1.5 K, and found that there are no crossing nor overlapping of the Te(I) and Te(II) peaks in the angle dependence in the ab plane. This makes the previous peak assignment revised: the hyperfine-coupling constants at two Te-NMR peaks are nearly isotropic. From the results of $H \parallel a$, the magnetic fluctuations along each axis R_a were derived. We found the predominance of the FM fluctuations along the a axis, which would be the properties inside the two-leg ladder along the a axis.

Acknowledgments The authors would like to thank Y. Yanase, S. Fujimoto, W. Knafo, K. Kaneko, G. Knebel, J.-P. Brison, S. Raymond, and J. Flouquet for their valuable discussions. This work was supported by the Kyoto University LTM Center, Grants-in-Aid for Scientific Research (Grant Nos. JP15H05745, JP17K14339, JP19K03726, JP16KK0106, JP19K14657, JP19H04696, JP20H00130, JP20KK0061, JP22H01168 and JP22H04933) from JSPS.

- 1) S. Ran, C. Eckberg, Q.-P. Ding, Y. Furukawa, T. Metz, S. R. Saha, I.-L. Liu, M. Zic, H. Kim, J. Paglione, and N. P. Butch, *Science* **365**, 684 (2019).
- 2) D. Aoki, A. Nakamura, F. Honda, D. Li, Y. Homma, Y. Shimizu, Y. J. Sato, G. Knebel, J.-P. Brison, A. Pourret, D. Braithwaite, G. Lapertot, Q. Niu, M. Valiska, H. Harima, and J. Flouquet, *Journal of the Physical Society of Japan* **88**, 043702 (2019).
- 3) K. Momma and F. Izumi, *J. Appl. Cryst.* **44**, 1272 (2011).
- 4) S. Ran, I.-L. Liu, Y. S. Eo, D. J. Campbell, P. M. Neves, W. T. Fuhrman, S. R. Saha, C. Eckberg, H. Kim, D. Graf, F. Balakirev, J. Singleton, J. Paglione, and N. P. Butch, *Nature Physics* **15**, 1250 (2019).
- 5) V. Hutanu, H. Deng, S. Ran, W. T. Fuhrman, H. Thoma, and N. P. Butch, *Acta Crystallographica Section B* **76**, 137 (2020).
- 6) D. Aoki, K. Ishida, and J. Flouquet, *Journal of the Physical Society of Japan* **88**, 022001 (2019).
- 7) S. S. Saxena, P. Agarwal, K. Ahilan, F. M. Grosche, R. K. W. Haselwimmer, M. J. Steiner, E. Pugh, I. R. Walker, S. R. Julian, P. Monthoux, G. G. Lonzarich, A. Huxley, I. Sheikin, D. Braithwaite, and J. Flouquet, *Nature* **406**, 587 (2000).
- 8) D. Aoki, A. Huxley, E. Ressouche, D. Braithwaite, J. Flouquet, J.-P. Brison, E. Lhotel, and C. Paulsen, *Nature* **413**, 613 (2001).
- 9) N. T. Huy, A. Gasparini, D. E. de Nijs, Y. Huang, J. C. P. Klaasse, T. Gortenmulder, A. de Visser, A. Hamann, T. Görlach, and H. v. Löhneysen, *Phys. Rev. Lett.* **99**, 067006 (2007).
- 10) D. Braithwaite, M. Vališka, G. Knebel, G. Lapertot, J.-P. Brison, A. Pourret, M. E. Zhitomirsky, J. Flouquet, F. Honda, and D. Aoki, *Communications Physics* **2**, 147 (2019).
- 11) S. M. Thomas, F. B. Santos, M. H. Christensen, T. Asaba, F. Ronning, J. D. Thompson, E. D. Bauer, R. M. Fernandes, G. Fabbri, and P. F. S. Rosa, *Science Advances* **6**, (2020).
- 12) C. Duan, K. Sasmal, M. B. Maple, A. Podlesnyak, J.-X. Zhu, Q. Si, and P. Dai, *Phys. Rev. Lett.* **125**, 237003 (2020).
- 13) W. Knafo, G. Knebel, P. Steffens, K. Kaneko, A. Rosuel, J.-P. Brison, J. Flouquet, D. Aoki, G. Lapertot, and S. Raymond, *Phys. Rev. B* **104**, L100409 (2021).
- 14) Y. Tokunaga, H. Sakai, S. Kambe, T. Hattori, N. Higa, G. Nakamine, S. Kitagawa, K. Ishida, A. Nakamura, Y. Shimizu, Y. Homma, D. Li, F. Honda, and D. Aoki, *Journal of the Physical Society of Japan* **88**, 073701 (2019).
- 15) G. Nakamine, S. Kitagawa, K. Ishida, Y. Tokunaga, H. Sakai, S. Kambe, A. Nakamura, Y. Shimizu, Y. Homma, D. Li, F. Honda, and D. Aoki, *Journal of the Physical Society of Japan* **88**, 113703 (2019).
- 16) G. Nakamine, K. Kinjo, S. Kitagawa, K. Ishida, Y. Tokunaga, H. Sakai, S. Kambe, A. Nakamura, Y. Shimizu, Y. Homma, D. Li, F. Honda, and D. Aoki, *Phys. Rev. B* **103**, L100503 (2021).
- 17) G. Nakamine, K. Kinjo, S. Kitagawa, K. Ishida, Y. Tokunaga, H. Sakai, S. Kambe, A. Nakamura, Y. Shimizu, Y. Homma, D. Li, F. Honda, and D. Aoki, *Journal of the Physical Society of Japan* **90**, 064709 (2021).
- 18) D. Li, A. Nakamura, F. Honda, Y. J. Sato, Y. Homma, Y. Shimizu, J. Ishizuka, Y. Yanase, G. Knebel, J. Flouquet, and D. Aoki, *Journal of the Physical Society of Japan* **90**, 073703 (2021).
- 19) Y. Tokunaga, H. Sakai, S. Kambe, Y. Haga, Y. Tokiwa, P. Opletal, H. Fujibayashi, K. Kinjo, S. Kitagawa, K. Ishida, A. Nakamura, Y. Shimizu, Y. Homma, D. Li, F. Honda, and D. Aoki, *Journal of the Physical Society of Japan* **91**, (2022).
- 20) Y. Haga, P. Opletal, Y. Tokiwa, E. Yamamoto, Y. Tokunaga, S. Kambe, and H. Sakai, *Journal of Physics: Condensed Matter* **34**, 175601 (2022).
- 21) K. Willa, F. Hardy, D. Aoki, D. Li, P. Wiccki, G. Lapertot, and C. Meingast, *Physical Review B* **104**, (2021).
- 22) S. Sundar, S. Gheidi, K. Akintola, A. M. Côté, S. R. Dunsiger, S. Ran, N. P. Butch, S. R. Saha, J. Paglione, and J. E. Sonier, *Phys. Rev. B* **100**, 140502 (2019).
- 23) S. Kambe, H. Sakai, Y. Tokunaga, and R. E. Walstedt, *Physical Review B* **82**, (2010).
- 24) D. V. Ambika, Q.-P. Ding, K. Rana, C. E. Frank, E. L. Green, S. Ran, N. P. Butch, and Y. Furukawa, *Physical Review B* **105**, (2022).
- 25) T. Kohara, Y. Kohori, K. Asayama, Y. Kitaoka, M. Maple, and M. Torikachvili, *Solid State Communications* **59**, 603 (1986).
- 26) M. Lee, G. F. Moores, Y.-Q. Song, W. P. Halperin, W. W. Kim, and G. R. Stewart, *Phys. Rev. B* **48**, 7392 (1993).
- 27) M. Kyogaku, Y. Kitaoka, K. Asayama, C. Geibel, C. Schank, and F. Steglich, *Journal of the Physical Society of Japan* **62**, 4016 (1993).
- 28) Y. Ihara, T. Hattori, K. Ishida, Y. Nakai, E. Osaki, K. Deguchi, N. K. Sato, and I. Satoh, *Phys. Rev. Lett.* **105**, 206403 (2010).
- 29) T. Hattori, Y. Ihara, Y. Nakai, K. Ishida, Y. Tada, S. Fujimoto, N. Kawakami, E. Osaki, K. Deguchi, N. K. Sato, and I. Satoh, *Phys. Rev. Lett.* **108**, 066403 (2012).
- 30) K. Karube, T. Hattori, S. Kitagawa, K. Ishida, N. Kimura, and T. Komatsubara, *Phys. Rev. B* **86**, (2012).